

ZMYM3 May Promote Cell Proliferation in Small Cell Lung Carcinoma

Noritaka Kudo^{1,2}, Shinji Kudoh¹, Akira Matsuo¹, Yamato Motooka³ and Takaaki Ito^{1,4}

¹Department of Pathology and Experimental Medicine, Kumamoto University Graduate School of Medical Sciences, 1–1–1 Honjo, Chuo-ku, Kumamoto 860–8556, Japan, ²Department of Pathology, The University of Tokyo, 7–3–1 Hongo, Bunkyo-ku, Tokyo 113–0033, Japan, ³Department of Thoracic Surgery, Kumamoto University Graduate School of Medical Sciences, 1–1–1 Honjo, Chuo-ku, Kumamoto 860–8556, Japan and ⁴Department of Medical Technology, Kumamoto Health Science University Faculty of Health Science, Izumi 325, Kita-ku, Kumamoto 861–5598, Japan

Received January 19, 2021; accepted August 16, 2021; published online October 2, 2021

Zinc finger, myeloproliferative, and mental retardation-type containing 3 (ZMYM3) is a highly conserved protein among vertebrates. Although it promotes DNA repair and moderate histone acetylation, the other functions of ZMYM3 remain unclear. We herein examined the physiological functions of ZMYM3 in human lung cancer using a ZMYM3-knockdown small cell lung cancer (SCLC) cell line. ZMYM3-knockdown SCLC cells grew slowly and the Ki-67 labeling index was lower in ZMYM3-knockdown cells than in mock cells. The subcutaneous tumors that formed after xenotransplantation into immunodeficient mice were slightly smaller in the ZMYM3-knockdown group than in the mock group. Furthermore, public RNA-sequencing data analyses showed similar RNA profiles between ZMYM3 and some cell proliferation markers. These results indicate that ZMYM3 promotes cell proliferation in human lung carcinomas, particularly SCLC.

Key words: ZMYM3, immunohistochemistry, mouse tissues, lung carcinoma, cell proliferation

I. Introduction

Lung cancer is a leading cause of cancer death [36]. Despite rapid advances in drug development and surgical procedures, current treatments for lung cancer, either small cell lung carcinoma (SCLC) or non-small cell lung carcinoma (NSCLC), do not achieve satisfactory outcomes [2, 18, 36]. To overcome the difficulties associated with treatments and elucidate the mechanisms underlying cell proliferation and differentiation in lung cancers, further analyses of molecular targets are needed.

Zinc finger, myeloproliferative, and mental retardation-type containing 3 (ZMYM3), also known as

DXS6673E, *ZNF261*, *ZNF198L2*, and *KIAA0385*, maps to Xq13.1, has the longest short tandem repeat (STR), a GA/32 dinucleotide repeat, in its 5' untranslated region (UTR) specifically in humans, and is evolutionarily conserved from *Drosophila melanogaster* to *Homo sapiens* [27, 33, 42]. Although ZMYM3 expression patterns have not yet been examined in detail, expression levels were previously shown to be the highest in the brain [42]. ZMYM3 moderates histone acetylation as a component of the HDAC2/BHC110-containing complex [14]. ZMYM3 is suppressed by the direct binding of BMI1 to the ZMYM3 promoter region, and the *c-fos* pathway is then activated by histone H3 acetylation [35]. ZMYM3 interacts with histone H2A/H2AX, which recruits ZMYM3 to damaged chromatin [24]. At damaged sites, ZMYM3 facilitates the accumulation of BRCA1 and promotes DNA repair by homologous recombination via interactions with the BRCA1-A subcomplex members, RAP80, ABRA1, and BRE [24]. *Zmym3*-knockout in adult male mice using the

Correspondence to: Takaaki Ito, MD, DMSc, Department of Pathology and Experimental Medicine, Kumamoto University Graduate School of Medical Sciences, 1–1–1 Honjo, Chuo-ku, Kumamoto 860–8556, Japan / Department of Medical Technology, Kumamoto Health Science University Faculty of Health Science, Izumi 325, Kita-ku, Kumamoto 861–5598, Japan. E-mail: takaito@kumamoto-u.ac.jp / itou-ta@kumamoto-hsu.ac.jp

CRISPR-Cas9 system has been shown to arrest spermatogenesis at metaphase of meiosis I [17]. *ZMYM3* has been implicated in the development of several mental disorders and neoplasms. *ZMYM3* was originally identified as a candidate gene of X-linked intellectual disability, and the translocation t(X; 13)(q13, q31) in the 5' UTR of *ZMYM3* was detected in a female case [42]. In male cases of X-linked intellectual disability, a missense mutation was found in exon 7 of *ZMYM3* [30]. *ZMYM3* is also one of the top candidate master regulators of Alzheimer's disease, and its expression levels were reduced in severe cases [5]. Some alterations to STRs in the 5' UTR of *ZMYM3* may be related to schizophrenia and bipolar disorder [3, 4]. Gene mutations have been reported in some neoplasms, such as prostate cancer, chronic lymphocytic leukemia, medulloblastoma (subgroup 4), and Ewing sarcoma, and were identified as missense mutations (prostate cancer, chronic lymphocytic leukemia, and medulloblastoma), nonsense mutations (prostate cancer, chronic lymphocytic leukemia, and medulloblastoma), and indels (prostate cancer, chronic lymphocytic leukemia, and Ewing sarcoma) [1, 31, 39, 43]. However, the relationships between many types of cancers, including lung cancer, and the expression of *ZMYM3* remain unclear.

In the present study, we investigated the expression patterns and functions of *ZMYM3* in human lung carcinomas, particularly SCLC. Its expression was assessed in human lung cancer cell lines by immunoblotting and in formalin-fixed paraffin-embedded lung cancer tissues by immunostaining. *ZMYM3* knockdown experiments on an SCLC cell line and public RNA-sequencing data analyses of human lung carcinoma were also performed to elucidate the functions of *ZMYM3* in lung cancer.

II. Materials and Methods

Cell lines and culture

Thirteen lung cancer cell lines were used in the present study: 7 SCLC cell lines (NCI-H69, NCI-H889, SBC-1, H69AR, NCI-H1688, SBC-3, and SBC-5), 3 adenocarcinoma (ADC) cell lines (A549, NCI-H358, and NCI-H1975), and 3 squamous cell carcinoma (SQC) cell lines (NCI-H226, NCI-H2170, and H15 (HCC15)) [8, 9, 12, 13, 19, 21, 23, 25]. The SBC-1, -3, and -5 and A549 cell lines were purchased from the Japan Collection of Research Bioresources Cell Bank (Osaka, Japan) and the H15 cell line was generously provided by Dr. Makoto Suzuki (Kumamoto University, Kumamoto, Japan). Other cell lines were purchased from the American Type Culture Collection (Manassas, VA, USA).

We mainly used the SCLC cell line, SBC-3, in the present study. SBC-3 cells were cultured in Eagle's minimal essential medium with L-glutamine (cat# 051-07615; Fujifilm Wako Pure Chemical Corporation, Osaka, Japan) supplemented with 10% fetal bovine serum, 100 U/mL potassium penicillin G (cat# 26239-42; Nacalai Tesque,

Inc., Kyoto, Japan), and 100 µg/mL streptomycin sulfate (cat# 32204-92; Nacalai Tesque, Inc.). Cultures were incubated at 37°C in the presence of 5% CO₂.

Tissue samples

Tissue samples of adult human lung tumors, ADC (n = 26), SQC (n = 32), and SCLC (n = 15), were surgically resected at the Department of Thoracic Surgery of Kumamoto University Hospital. Histological diagnoses were reached according to the criteria of the World Health Organization [41]. The present study followed the guidelines of the Ethics Committee of Kumamoto University.

In addition to tissue samples of human lung cancers, we analyzed multiple tissues from adult female ICR mice (Japan SLC, Fukuoka, Japan) and tissue samples of the tumors that formed after the xenotransplantation of tumor cells.

ZMYM3-knockdown by RNA interference

The *ZMYM3* gene was knocked down by RNA interference in the SCLC line, SBC-3. *ZMYM3* short-hairpin RNA (shRNA) plasmids (Sure Silencing shRNA Plasmid Puromycin Human *ZMYM3*; cat# 336314 KH07693P; Qiagen, Hilden, Germany) were transfected in SBC-3 cells by electroporation. The sequence of the plasmids was AGTGTAGACTTCCTCTTTGAT. Negative control shRNA had the following scrambled artificial sequence: GGAATCTCATTCGATGCATAC, which did not match any of those from humans or mice. Transfected cells were selected by adding puromycin at a final concentration of 2 µg/mL to the medium described above. After colonies had formed, they were isolated with cloning cylinders and individually picked up from dishes.

Immunohistochemistry and immunocytochemistry

The tissue samples of adult human lung tumors were fixed in 10% neutral buffered formalin, and those from mice and tumors that formed after xenotransplantation were fixed in phosphate-buffered 4% paraformaldehyde (PFA). They were embedded in paraffin, sliced into 3-µm-thick sections with a microtome (Leica SM2010R—Sliding Microtome; Leica biosystems, Wetzlar, Germany), and mounted on adhesive-coated slides (Frontier Green FRC-05; Matsunami Glass Ind., Ltd.). Sections were then deparaffinized and rehydrated through a xylene-ethanol series.

Cells were cultured on a 4-well chamber slide (Nunc Lab-Tek II Chamber Slide System; cat# 154526; Thermo Fisher Scientific). After washing with phosphate-buffered saline (PBS) for 5 min, cells were dried for 30 min and fixed in phosphate-buffered 4% PFA for 1 hr.

Antigens were activated with an autoclave at 121°C for 15 min. As the retrieval solution, citrate buffer solution, pH 7.0, was used for *ZMYM3* immunostaining and Tris-EDTA buffer solution, pH 9.0, for Ki-67 immunostaining. Endogenous peroxidase blockage was performed

Table 1. Details of the primary antibodies used for immunohistochemistry and western blotting in the present study

Target Molecule	Clone	Host Species	Clonality	Catalog Number	Manufacturer (Headquarters)	Dilution		Reference
						IHC, ICC	IB	
ZMYM3		Rabbit	Polyclonal	ab84507	Abcam (Cambridge, UK)	1:100	1:2000	N/A
Ki-67		Mouse	Monoclonal	M7240	Dako (Glostrup, Denmark)	1:100		[37]
Cyclin D1	SP4	Rabbit	Monoclonal	RM-9104-S1	Thermo Fisher Scientific (Waltham, MA, USA)		1:1000	[44]
pPH3	Ser10	Rabbit	Polyclonal	06-570	Merck KGaA (Darmstadt, Germany)		1:1000	[20]
CASP3		Rabbit	Polyclonal	9662	Cell Signaling Technology (Danvers, MA, USA)		1:5000	[32]
Cleaved CASP3	Asp175	Rabbit	Polyclonal	9661	Cell Signaling Technology		1:100	[38]
β-actin	AC-15	Mouse	Monoclonal	A5441	Sigma-Aldrich (St. Louis, MO, USA)		1:40000	[32]

pPH3: phosphor-histone H3, CASP3: caspase 3, IHC: immunohistochemistry, ICC: immunocytochemistry, IB: immunoblotting, N/A: not available.

with 0.3% H₂O₂ in methanol at room temperature for 30 min. Non-specific protein binding was blocked with 5% skim milk in Tris-HCl buffer at room temperature for 20 min. The primary antibodies were diluted with an antibody diluent (cat# S2022; Dako, Glostrup, Denmark), applied to sections, and incubated in a humid chamber overnight at 4°C. Details on the primary antibodies used in the present study are summarized in Table 1. As secondary antibodies, an anti-rabbit antibody linked with horseradish peroxidase (HRP) (cat# K4003; Dako) was used for ZMYM3 immunostaining and a HRP-linked anti-mouse antibody (cat# K4001; Dako) for Ki-67 immunostaining. After washing, the secondary antibodies were applied to the sections and incubated in a humid chamber at room temperature for one hour. Immunolabeled sites were detected with 3,3'-diaminobenzidine (DAB) (cat# K3468; Dako). Nuclei in sections were counter-stained with hematoxylin for 1 min, and washed in running tap water for 5 min. Sections were then dehydrated through an ethanol-xylene series and mounted in malinol (cat# 20093; Muto Pure Chemical Co., Ltd., Tokyo, Japan).

The negative control was obtained by substituting PBS for the primary antibodies. The other procedures were conducted in the same manner as described above.

Ki-67 labeling index

The Ki-67 labeling index was defined as the percentage of Ki-67-positive nuclei. We used tissue and cell samples immunostained for Ki-67 described above to assess the Ki-67 labeling index. In each sample, 500 cells each were counted in 5 microscopic fields. Any staining of nuclei in cells, regardless of the staining intensity, was considered to be positive for Ki-67.

BrdU cell proliferation assay

Cells were cultured on a 4-well chamber slide (Thermo Fisher Scientific). 5-Bromo-2'-deoxyuridine

(BrdU) was added to the cell culture medium after mechanical sterilization at a final concentration of 1 mg/mL. Cells were cultured in medium supplemented with BrdU for 2 hr. After washing with PBS for 5 min, cells were dried for 30 min and fixed in phosphate-buffered 4% PFA for 1 hr. Antigens were activated with 0.4% pepsin (cat# 24-0940-2; Sigma-Aldrich, St. Louis, MO, USA) solution in 0.1 mol/L HCl for 30 min. The other procedures were conducted in the same manner as the immunocytological experiment. An anti-BrdU rat antibody (dilution 1:2000; Nichirei Bioscience, Tokyo, Japan) was used as the primary antibody and a peroxidase-labeled anti-rat antibody (MAX-PO; Nichirei) as the secondary antibody. In each sample, 500 cells each were counted from 5 microscopic fields.

Immunoblotting (Western blotting)

Cell samples were lysed in cell lysis buffer (20 mM Tris-HCl, 150 mM NaCl, 1 mM ethylenediaminetetraacetic acid, 1 mM ethylene glycol tetraacetic acid, 2.5 mM sodium pyrophosphate, 1 mM β-glycerophosphate, 1% Triton X-100, 0.1% SDS, 0.5% sodium deoxycholate, and 0.5% distilled water) supplemented with 1 mmol/L sodium orthovanadate, 1 mmol/L phenylmethanesulfonyl fluoride and protease inhibitor cocktail (cOmplete; cat# 11697498001; F. Hoffmann-La Roche, Basel, Switzerland). Proteins in the cell lysate were separated by electrophoresis on an agarose gel. Separated proteins were electrophoretically transferred to a nitrocellulose membrane (Amersham Protran Premium 0.45 μm NC; cat# 10600003; GE Healthcare, Chicago, Ill, USA). The non-specific background was blocked with skim milk in tris-buffered saline with 0.1% Tween 20 at room temperature for 1 hr. The membrane was immunoblotted with primary antibodies at 4°C overnight. Details on the primary antibodies used in the present study are summarized in Table 1. After washing, the membrane was incubated with the secondary antibodies at room temperature for 90 min. The following antibodies

were used as the secondary antibodies at a 1:10000 dilution according to the host species of the primary antibodies: a HRP-linked anti-rabbit antibody (cat# 7074; Cell Signaling Technology, Danvers, MA, USA) and a HRP-linked anti-mouse antibody (cat# 7076; Cell Signaling Technology). Immunoreactive sites were detected using an enhanced chemiluminescence system with Western Lightning *Plus* Enhanced Chemiluminescence Substrates for Western Blotting (for β -actin; PerkinElmer, Waltham, MA, USA) or Amersham ECL Prime Western Blotting Detection Reagent (for the others; GE Healthcare), and visualized by exposing the membrane to an X-ray film (Fuji Medical X-ray Film Super RX; Fujifilm Corporation, Tokyo, Japan). β -actin was used as the loading control. Blots were stripped and reprobed with other antibodies or the anti- β -actin antibody.

Cell counting assay

Cells were seeded at 50,000 cells/well on 6-well plates (cat# 140675; Thermo Fisher Scientific). They were then harvested by trypsinization every day up to 5 days of culture and manually counted with a hemocytometer (Burker-Turk; Sunlead Glass Corp., Saitama, Japan) after trypan blue staining. At each time point, 5 samples were counted in each cell clone.

Induction of apoptosis

Etoposide was used to induce apoptosis [29]. We initially examined the optimal concentration and retention time of etoposide for the induction of apoptosis. Cells were seeded at 200,000 cells/well on 6-well plates (Thermo Fisher Scientific). One day after seeding, etoposide was added to the cell culture medium at concentrations of 0, 100 and 500 μ M. Viable cells were manually counted 0, 6, 24, 48, and 72 hr after the addition of etoposide in the same manner as the cell growth curve experiment. At each time point, 5 samples were counted at each concentration of etoposide. Based on the results obtained, we induced apoptosis in the present study by adding etoposide at a concentration of 500 μ M to the cell culture medium for 24 hr.

Flow cytometry

After the induction of apoptosis, cells were harvested by trypsinization from culture dishes with the supernatant and filtered through a 100- μ m cell strainer followed by a 40- μ m cell strainer. Cells were resuspended in 100 μ L of annexin-binding buffer (10 mM HEPES, 140 mM NaCl, and 2.5 mM CaCl_2 , pH 7.4) (cat# V13246; Thermo Fisher Scientific) and double-stained with 5 μ L of annexin V conjugated with Alexa Fluor 488 (cat# A13201; Thermo Fisher Scientific) and 2 μ L of 100 μ g/mL propidium iodide (PI) (cat# P4170-100MG; Sigma-Aldrich) in water for 15 min. After the addition of 400 μ L of annexin-binding buffer to the cell suspension, a flow cytometry analysis was conducted with the cell sorter, SH800S (Sony Imaging Products & Solutions Inc., Tokyo, Japan) and FlowJo software

(version 10.7.1; FlowJo LLC, Ashland, OR, USA). Using annexin V/PI double staining, annexin V single-positive cells were estimated as early apoptotic cells and annexin V/PI double-positive cells as late apoptotic cells [22, 28, 34]. We also examined the induction of apoptosis using light scattering, and cells in the population with low forward and high side scatters were estimated as apoptotic cells [7, 34].

Xenotransplantation

A total of 1.0×10^6 cells were mixed with PBS and injected into the subcutaneous tissues of 13-week-old female immunodeficient mice, *Rag2* and *Jak3* double knockout mice (a generous gift from Prof. S. Okada, Kumamoto University). Four weeks after the injection, mice were sacrificed and the subcutaneous tumors that formed after the injection were excised. The length, width, and height of subcutaneous tumors were measured and the approximate volume of tumors was calculated using the following formula: (tumor volume [mm^3]) = $\pi/6 \times$ (length [mm]) \times (width [mm]) \times (height [mm]), where $\pi \approx 3.14$. Tumors were then histologically examined.

Terminal nucleotidyl transferase (TdT)-mediated dUTP-biotin nick end-labeling (TUNEL) assay

An *In situ* Apoptosis Detection Kit (cat# MK500; Takara Bio Inc., Shiga, Japan) was used in this experiment. After deparaffinization and endogenous peroxidase inactivation, 50 μ L of the labeling reaction mixture (5 μ L of TdT enzyme plus 45 μ L of labeling safe buffer) was applied to slides. Slides were then incubated in a humid chamber at 37°C for 60–90 min. After the application of 70 μ L of the anti-fluorescein isothiocyanate HRP conjugate, slides were incubated at 37°C for 30 min. Immunolabeled sites were detected with DAB, and slides were counter-stained with methyl green.

Public RNA-sequencing data

We downloaded public RNA-sequencing data from cBioPortal for Cancer Genomics (<https://www.cbioportal.org/datasets>) on three histological subtypes of lung carcinoma: ADC (Lung Adenocarcinoma (TCGA, Firehose Legacy); https://www.cbioportal.org/study/summary?id=luad_tega), SQC (Lung Squamous Cell Carcinoma (TCGA, Firehose Legacy); https://www.cbioportal.org/study/summary?id=lusc_tega), and SCLC (Small Cell Lung Cancer (U Cologne, Nature 2015); https://www.cbioportal.org/study/summary?id=sclc_ucologne_2015) [10]. The sample numbers of these RNA-sequencing data on ADC, SQC and SCLC were $n = 517, 501,$ and $81,$ respectively. Data on ADC and SQC were provided as z-scores (log RNA Seq V2 RSEM), and those on SCLC as z-scores (log RNA Seq FPKM). The RNAs examined in this experiment were *ZMYM3*, cyclin D1 (*CCND1*, a cell cycle regulatory protein), and the following cell proliferation markers: marker of proliferation Ki-67 (*MKI67*), minichromosome mainte-

nance complex component 2 (*MCM2*), *MCM7*, DNA topoisomerase II alpha (*TOP2A*), and proliferating cell nuclear antigen (*PCNA*) [6, 11, 15, 16, 26, 40].

Statistical analysis

The Shapiro-Wilk normality test was used to examine normality. When data followed a normal distribution, after the confirmation of the equality of two variances by the *F*-test, the Student's *t*-test was used. When data did not follow a normal distribution, the Mann-Whitney's *U* test was used. Due to the non-parametricity of data in the present study, Spearman's rank correlation coefficient (ρ) was employed to investigate relationships. We regarded *p*-values < 0.05 as significant. The software used for these analyses was R for windows (Version 3.6.1; R foundation for Statistical Computing, Vienna, Austria).

III. Results

ZMYM3 immunostaining was performed to detect the expression of ZMYM3 in human lung carcinomas. The lung cancers examined positively stained for ZMYM3, regardless of the histological subtypes (Fig. 1B–D, Table 2). In the normal tissues surrounding tumors, epithelial cells in the bronchioles and some alveolar epithelial cells, which appeared to be type II, were positively stained (Fig. 1A). Differences in stainability were unclear between ciliated and club cells. In the majority of specimens, the tissues of carcinomas stained more strongly than the normal tissues surrounding carcinomas (Table 2).

The expression of ZMYM3 was examined in lung cancer cell lines by immunoblotting and the majority of the cell lines examined were positive for ZMYM3, except for H15 (Fig. 1E).

To clarify the functional significance of ZMYM3 in lung cancer, *ZMYM3* was knocked down in the SCLC cell line, SBC-3 by RNA interference using shRNA. Knockdown was confirmed by immunoblotting and immunocytochemistry (Fig. 2A, E). We used one *ZMYM3*-knockdown cell clone and one mock in the present study. The effects of the knockdown of *ZMYM3* on cell proliferative activities were assessed by immunoblotting (Fig. 2B). The expression of cyclin D1 in the *ZMYM3*-knockdown cell clone was slightly lower than that in the mock (Fig. 2B). However, no marked differences were observed in phospho-histone H3 expression levels between *ZMYM3*-knockdown cells

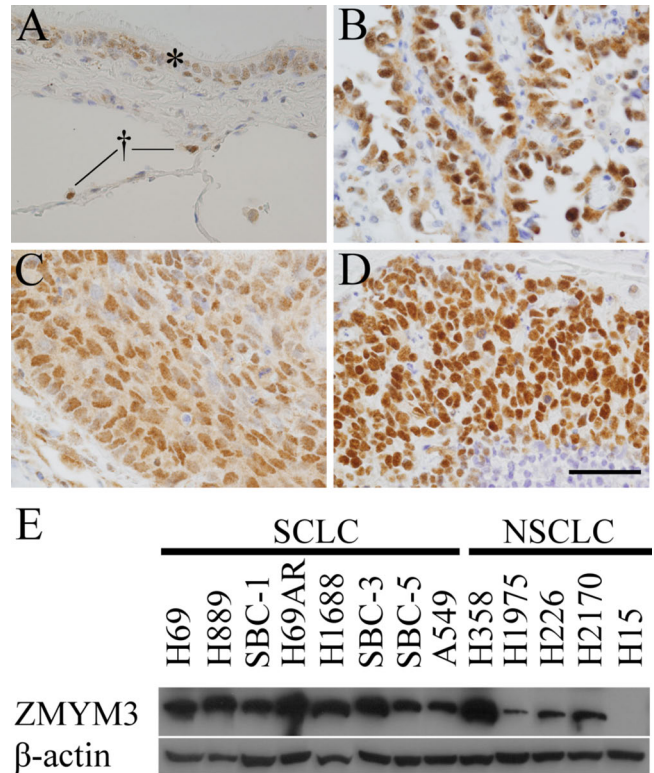


Fig. 1. (A–D) ZMYM3 immunostaining in human lung tissues and lung cancers. (A) In normal tissues around tumors, bronchiolar epithelial cells (asterisk) and some alveolar cells (dagger), which appeared to be type II, were stained in nuclei. (B–D) In lung carcinomas, all 3 histological types: adenocarcinoma (ADC) (B), squamous cell carcinoma (SQC) (C), and small cell lung carcinoma (SCLC) (D), were strongly stained in nuclei. Original magnification: $\times 400$. Bar = 50 μ m. (E) Immunoblotting was also performed on 13 lung cancer cell lines: 7 SCLC cell lines (H69, H889, SBC-1, H69AR, H1688, SBC-3, and SBC-5) and 6 non-SCLC (NSCLC) cell lines (A549, H358, H1975, H226, H2170, and H15). All cell lines, except for H15, expressed ZMYM3. The prefix “NCI-” was omitted. β -actin was used as an internal control.

and mock cells (Fig. 2B). We also examined the effects of the *ZMYM3*-knockdown on apoptotic activities by immunoblotting under the induction of apoptosis by etoposide (Fig. 2C). The optimal concentration and retention time of etoposide for the induction of apoptosis were investigated and confirmed before this experiment (Supplementary Fig. S2A). No marked differences were noted in the expression of caspase 3 between the *ZMYM3*-knockdown

Table 2. Comparison of staining intensity of ZMYM3 between lung carcinoma cells and normal bronchoalveolar epithelial cells

Histological subtypes (Total number of specimens)	(–)	(±)	(+)	(++)	The percentage of (++) [%]
Adenocarcinoma (26)	0	0	4	22	84.62
Squamous cell lung carcinoma (32)	0	1	6	25	78.13
Small cell lung carcinoma (15)	0	0	0	15	100

The staining intensity of ZMYM3-positive normal bronchoalveolar epithelial cells was regarded as (+). (–) no stainability, (±) weaker, (+) same, (++) stronger.

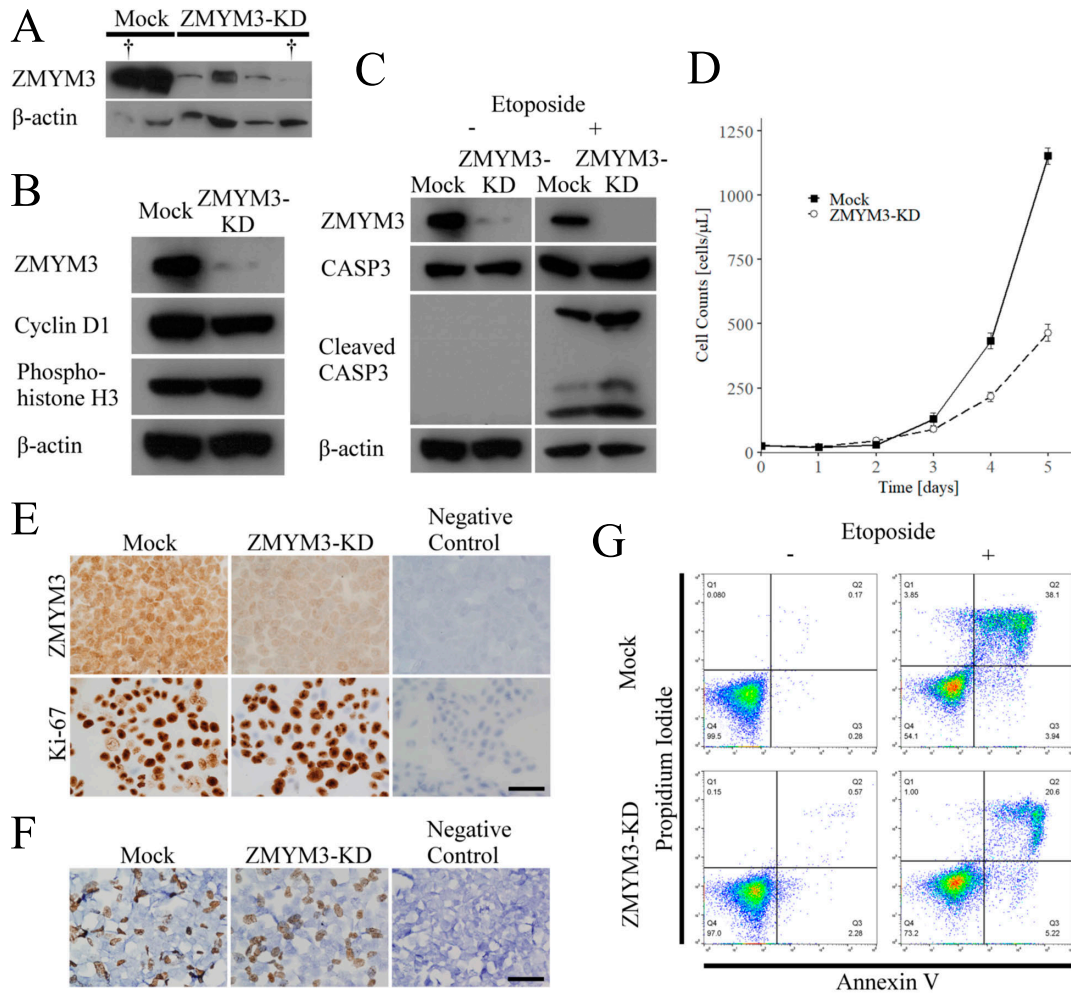


Fig. 2. (A) The knockdown of *ZMYM3* in the small cell lung carcinoma (SCLC) cell line, SBC-3. An immunoblotting analysis confirmed the decreased expression of *ZMYM3*. Daggers represent the cell clones used in the present study. β -actin was used as a loading control. (B) Immunoblotting of *ZMYM3* knockdown cells and the negative control, mock cells, with a focus on cell proliferation. Cyclin D1 expression was slightly decreased in *ZMYM3*-knockdown cells. (C) Immunoblotting of *ZMYM3*-knockdown cells and mock cells with a focus on apoptosis. Under the induction of apoptosis by etoposide, cleaved caspase 3 increased in *ZMYM3*-knockdown cells. (D) Cell growth curve of the *ZMYM3*-knockdown cell clone and the mock. On day five, the cell count was significantly lower for the *ZMYM3*-knockdown cell clone than for the mock (average 465.0 versus 1153.0, $p = 4.147 \times 10^{-7}$). (E) Immunohistochemistry for *ZMYM3* and Ki-67 in the *ZMYM3*-knockdown cell clone and the mock. Immunohistochemistry for *ZMYM3* also confirmed the decreased expression of *ZMYM3*. The Ki-67 labeling index was significantly lower in the *ZMYM3*-knockdown cell clone than in the mock (average 416.4 versus 432.6 per 500 cells, $p = 0.042$). (F) The BrdU cell proliferation assay on the *ZMYM3*-knockdown cell clone and the mock. No significant differences were observed between the *ZMYM3*-knockdown cell clone and the mock. (G) Analysis of apoptosis by flow cytometry using annexin V/propidium iodide. Annexin V single-positive cells represent early apoptosis cells, while annexin V/propidium iodide double-positive cells represent late apoptosis cells. Even under the induction of apoptosis by etoposide, no marked differences were observed in apoptotic activities between *ZMYM3*-knockdown cell clone and the mock. KD: knockdown, CASP3: caspase 3.

cell clone and the mock, regardless of the induction of apoptosis (Fig. 2C). However, the expression of cleaved caspase 3 was increased in the *ZMYM3*-knockdown cell clone under the induction of apoptosis (Fig. 2C).

Based on the results of cyclin D1 immunoblotting, the *ZMYM3*-knockdown appeared to suppress cell proliferation. We examined the proliferation of *ZMYM3*-knockdown cells and mock cells using a cell growth curve (Fig. 2D). The cell growth curve showed a reduction in the proliferation of *ZMYM3*-knockdown cells (Fig. 2D). On day 5, a significant difference was observed in the number of

ZMYM3-knockdown cells and mock cells (average 465.0 versus 1153.0, $t = 14.859$, $p = 4.147 \times 10^{-7}$). We also evaluated the cell proliferative activities of these cell clones by immunocytochemistry, the Ki-67 labeling index, and BrdU cell proliferation assay (Fig. 2E, F). The Ki-67 labeling indexes of *ZMYM3*-knockdown cells and mock cells were 83.3 and 86.5%, respectively. The count of Ki-67-positive nuclei per 500 *ZMYM3*-knockdown cells was significantly lower than that of mock cells (average 416.4 versus 432.6, $t = 2.425$, $p = 0.042$). However, the results of the BrdU cell proliferation assay revealed no significant

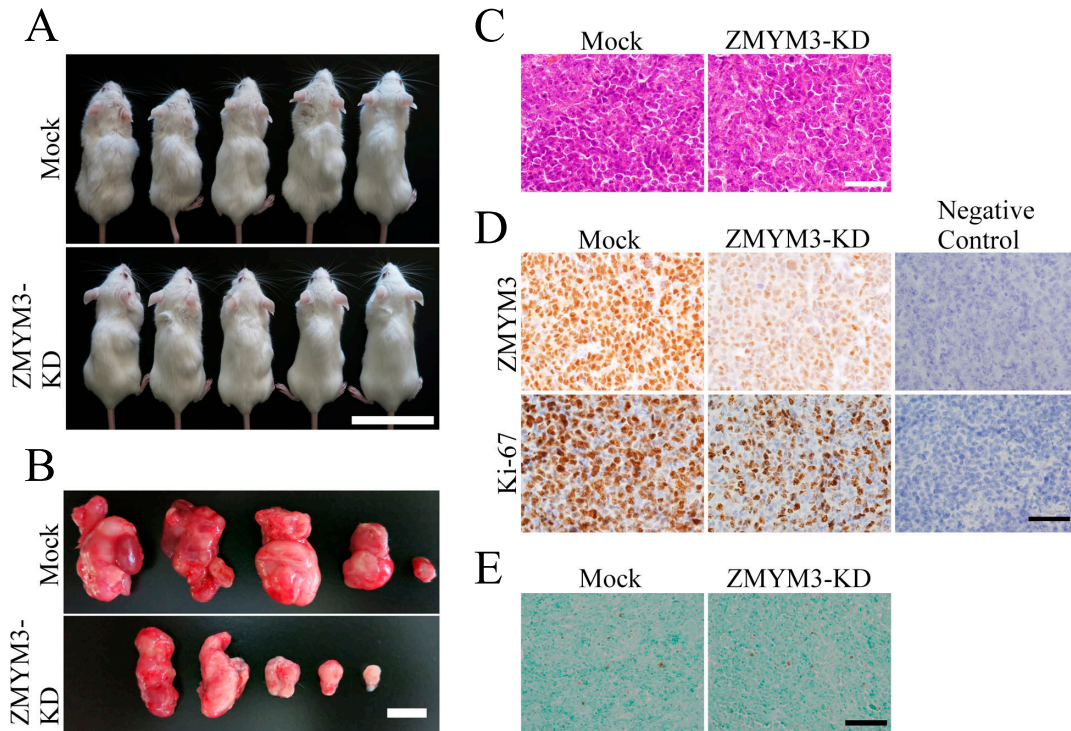


Fig. 3. Xenotransplantation of *ZMYM3*-knockdown cells and mock cells into the back skin of immunodeficient mice. (A) Tumors formed under the skin of mice. (B) The tumors of *ZMYM3*-knockdown cells were slightly smaller than those of mock cells. However, no significant differences were observed in volumes between *ZMYM3*-knockdown tumors and mock tumors (average 1181.5 versus 362.5, $p = 0.222$). (C) Hematoxylin-eosin staining of tumors. No significant morphological differences were observed between *ZMYM3*-knockdown tumors and mock tumors. Original magnification: $\times 400$. Bar = 50 μm . (D) *ZMYM3* and Ki-67 immunostaining in tumors. *ZMYM3* immunostaining revealed a decrease in *ZMYM3* expression in *ZMYM3*-knockdown cells. The Ki-67 labeling index was significantly lower in *ZMYM3*-knockdown cells than in mock cells (average 378.6 versus 350.8, $p = 0.025$). Original magnification: $\times 400$. Bar = 50 μm . (E) TUNEL assay of tumors. No significant differences were noted in apoptosis counts between *ZMYM3*-knockdown tumors and mock tumors (average 6.6 versus 9.0, $p = 0.373$). Original magnification: $\times 200$. Bar = 100 μm .

differences between the number of BrdU-positive cells per 500 *ZMYM3*-knockdown cells and that of mock cells (average 179.4 versus 192.2, $t = 1.002$, $p = 0.349$). Based on these results, we hypothesized that *ZMYM3* may promote cell proliferation. In *Zmym3* immunohistochemistry on normal mouse tissue, *Zmym3*-positive cells were observed in some actively proliferating regions, such as basal cells in the esophageal epithelium, the isthmus of the gastric gland, the intestinal cryptal epithelium, the germinal centers of the lymph nodes and the spleen, and the ovarian follicles (Supplementary Fig. S1).

To rule out the possibility that *ZMYM3* suppresses apoptosis in human lung cancer cells, we examined the apoptotic activities of *ZMYM3*-knockdown cells and mock cells by flow cytometry under the induction of apoptosis by etoposide. Twenty-four hours after the addition of 500 μM etoposide, a separate population formed with low forward and high side scatters, which indicated the induction of apoptosis (Supplementary Fig. S2B). Annexin V/PI double staining revealed the presence of early and late apoptotic cells (Fig. 2G). However, no significant differences were observed between the apoptotic activities of the *ZMYM3*-knockdown cell clone and the mock.

In further examinations, *ZMYM3*-knockdown cells and

mock cells were xenotransplanted into the subcutaneous tissues of immunodeficient mice. Four weeks after xenotransplantation, tumors formed in subcutaneous tissues (Fig. 3A). These tumors were resected and measured, and their volumes were estimated. *ZMYM3*-knockdown tumors were slightly smaller than mock tumors (average 1181.5 versus 362.5, $U = 19$, $p = 0.222$) (Fig. 3B). A histological examination with HE staining revealed no morphological differences between *ZMYM3*-knockdown cells and mock cells (Fig. 3C). Using *ZMYM3* immunohistochemistry, the effects of the *ZMYM3*-knockdown were reexamined in the tumors that formed after xenotransplantation (Fig. 3D). The Ki-67 labeling indexes of *ZMYM3*-knockdown cells and mock cells were 70.2 and 75.7%, respectively. The count of Ki-67 positive nuclei per 500 *ZMYM3*-knockdown cells was significantly lower than that of mock cells (average 350.8 versus 378.6, $t = 2.316$, $p = 0.025$) (Fig. 3D). In the TUNEL assay, no significant differences were observed between apoptotic cell counts per 500 *ZMYM3*-knockdown cells and that of mock cells (average 6.6 versus 9.0, $t = 0.944$, $p = 0.373$) (Fig. 3E). Regardless of the sizes of tumors, no marked differences were noted in morphology, necrosis, or apoptosis.

To clarify the relationships between *ZMYM3* and cell

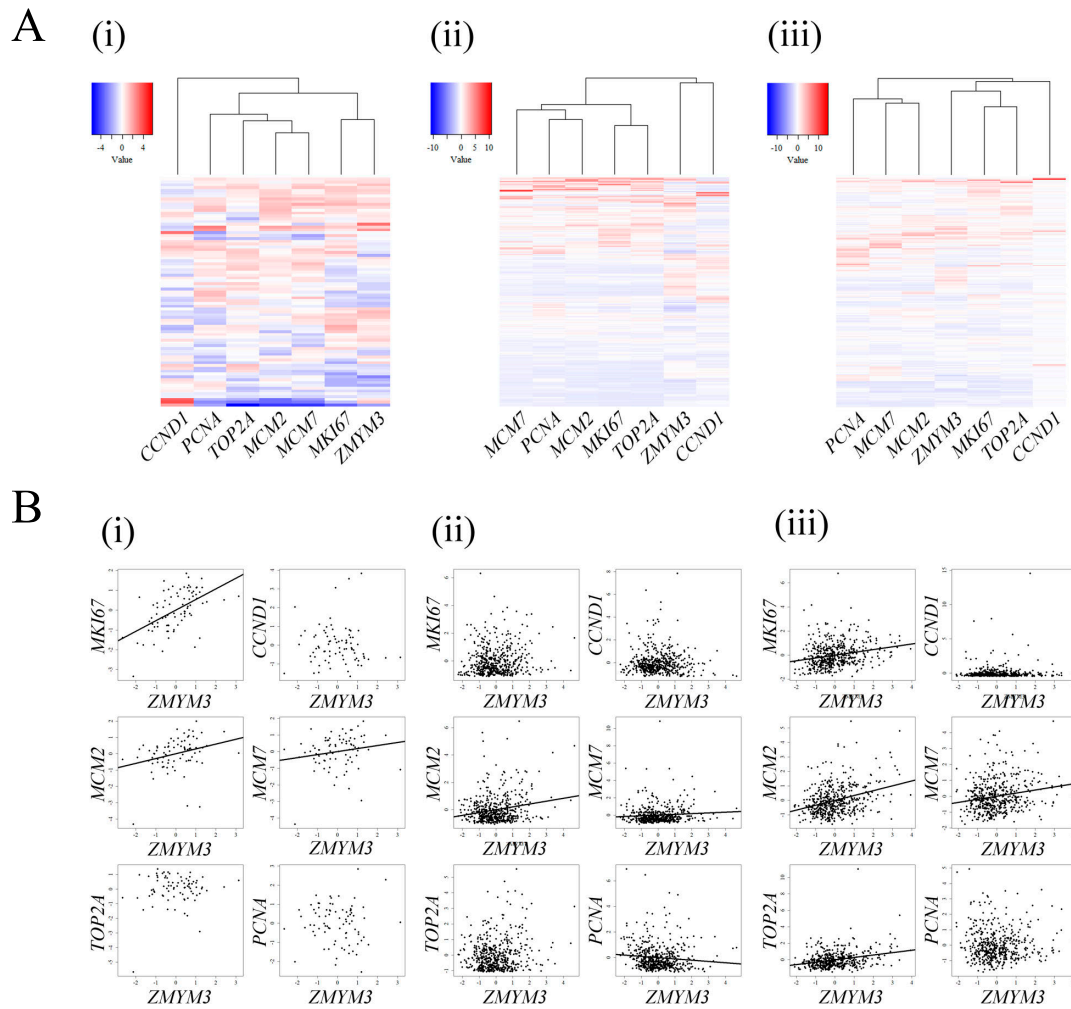


Fig. 4. (A) Heat maps of RNA profiles in three histological subtypes of lung carcinoma: small cell lung carcinoma (SCLC) (i), adenocarcinoma (ADC) (ii), squamous cell carcinoma (SQC) (iii). (i, iii) In the heat maps of SCLC and SQC, the expression profiles of *ZMYM3* were similar to those of cell proliferation markers (*MKI67*, *MCM2*, *MCM7*, *TOP2A*, and *PCNA*), but not to those of the cell cycle regulatory protein, *CCND1*. (ii) In contrast to SCLC and SQC, in the heat map of ADC, the similarity of expression profiles was weak between *ZMYM3* and cell proliferation markers. (B) Scatter diagrams of *ZMYM3* versus cell proliferation markers (*MKI67*, *CCND1*, *MCM2*, *MCM7*, *TOP2A*, and *PCNA*) in the three histological subtypes of lung carcinoma: SCLC (i), ADC (ii), and SQC (iii). From left to right, top to bottom: *ZMYM3* versus *MKI67*, *CCND1*, *MCM2*, *MCM7*, *TOP2A*, and *PCNA*. When correlations were observed, regression lines were added to scatter diagrams. (i) Positive correlations were observed between *ZMYM3* and *MKI67* ($\rho = 0.534$, $p = 2.894 \times 10^{-7}$), *MCM2* ($\rho = 0.346$, $p = 1.640 \times 10^{-3}$), and *MCM7* ($\rho = 0.227$, $p = 0.042$). (ii) Positive correlations were observed between *ZMYM3* and *MCM2* ($\rho = 0.098$, $p = 0.026$) and *MCM7* ($\rho = 0.099$, $p = 0.025$). A negative correlation was observed between *ZMYM3* and *PCNA* ($\rho = -0.150$, $p = 5.983 \times 10^{-4}$). (iii) Positive correlations were observed between *ZMYM3* and *MKI67* ($\rho = 0.264$, $p = 1.912 \times 10^{-9}$), *MCM2* ($\rho = 0.264$, $p = 2.090 \times 10^{-9}$), *MCM7* ($\rho = 0.176$, $p = 7.385 \times 10^{-5}$), and *TOP2A* ($\rho = 0.245$, $p = 2.773 \times 10^{-8}$).

proliferation in lung carcinoma, we analyzed the RNA profiles of three histological subtypes of lung carcinoma, SCLC, ADC, and SQC, using public RNA-sequencing data sets. *ZMYM3* was compared with the cell cycle regulatory protein, *CCND1*, and five cell proliferation markers, *MKI67*, *MCM2*, *MCM7*, *TOP2A*, and *PCNA*. The heat map of SCLC showed that the *ZMYM3* profile roughly resembled those of the five cell proliferation markers, particularly *MKI67*, but not that of *CCND1* (Fig. 4A(i)). The heat map of SQC showed a similar pattern to that of SCLC (Fig. 4A(iii)). In the heat map of ADC, only small similarities were observed between *ZMYM3* and the five cell proliferation markers (Fig. 4A(ii)). In SCLC, *ZMYM3* positively

correlated with *MKI67* ($\rho = 0.534$, $p = 2.894 \times 10^{-7}$), *MCM2* ($\rho = 0.346$, $p = 0.002$), and *MCM7* ($\rho = 0.227$, $p = 0.042$), but not with *TOP2A* ($\rho = 0.003$, $p = 0.980$), *PCNA* ($\rho = -0.104$, $p = 0.355$), or *CCND1* ($\rho = -0.115$, $p = 0.306$) (Fig. 4B(i)). In SQC, *ZMYM3* positively correlated with *MKI67* ($\rho = 0.264$, $p = 1.912 \times 10^{-9}$), *MCM2* ($\rho = 0.264$, $p = 2.090 \times 10^{-9}$), *MCM7* ($\rho = 0.176$, $p = 7.385 \times 10^{-5}$), and *TOP2A* ($\rho = 0.245$, $p = 2.773 \times 10^{-8}$), but not with *PCNA* ($\rho = -0.024$, $p = 0.595$) or *CCND1* ($\rho = 0.002$, $p = 0.966$) (Fig. 4B(iii)). In ADC, *ZMYM3* positively correlated with *MCM2* ($\rho = 0.098$, $p = 0.026$) and *MCM7* ($\rho = 0.098$, $p = 0.025$), and negatively correlated with *PCNA* ($\rho = -0.150$, $p = 5.983 \times 10^{-4}$), but did not correlate with *MKI67* (ρ

= 0.081, $p = 0.066$), *TOP2A* ($p = 0.041$, $p = 0.348$), or *CCND1* ($p = 0.029$, $p = 0.510$) (Fig. 4B(ii)).

IV. Discussion

To clarify ZMYM3 expression profiles in human cancers, we selected human lung cancer as an example. The staining intensity for ZMYM3 was slightly stronger in lung cancer tissues than in the non-neoplastic lung epithelial cells surrounding tumors regardless of the histological subtype. The up-regulated expression of ZMYM3 in lung cancer tissues suggested that ZMYM3 plays important roles, in cancer cells, such as cell proliferation, survival, and motility.

To elucidate the functional significance of ZMYM3 in lung cancer, we performed the knockdown of ZMYM3 in a SCLC cell line by RNA interference with shRNA. The growth of ZMYM3-knockdown cells was significantly slower than that of mock cells in the cell counting assay. Similarly, the subcutaneous tumors that formed after xenotransplantation into immunodeficient mice were slightly smaller in the ZMYM3-knockdown group than in the mock group. Ki-67 labeling indexes were also significantly lower in ZMYM3-knockdown cells than in mock cells under cell culture and xenotransplantation conditions. Consistent with these results, the expression of Cyclin D1 appeared to decrease in ZMYM3-knockdown cells in the immunoblotting analysis. In the BrdU cell proliferation assay, the scores of ZMYM3-knockdown cells were slightly smaller than those of mock cells. Based on these results, we hypothesized that ZMYM3 promoted cell proliferation in lung carcinomas. To examine this hypothesis, we conducted public RNA-sequencing data analyses of three histological subtypes of lung carcinoma, SCLC, ADC, and SQC. The heatmaps of SCLC and SQC, particularly SCLC, roughly resembled those of the five cell proliferation markers, *MKI67*, *MCM2*, *MCM7*, *TOP2A*, and *PCNA*, particularly *MKI67*. In addition, ZMYM3 and some cell proliferation markers positively correlated with each other in SCLC and SQC. These results were consistent with our hypothesis. Regarding the relationship between ZMYM3 and neoplasms, some mutations, including missense mutations, nonsense mutations, and indels, have been reported in some neoplasms, such as prostate cancer, chronic lymphocytic leukemia, medulloblastoma (subgroup 4), and Ewing sarcoma [1, 31, 39, 43]. To the best of our knowledge, ZMYM3 mutations in lung cancer have not yet been reported in the literature. In the public datasets used in the present study, only a few ZMYM3-mutated cases were detected; four out of 586 cases of ADC (three missense mutations and one truncating mutation), six out of 511 cases of SQC (five missense mutations and one truncating mutation), and three out of 120 cases of SCLC (three missense mutations); however, the significance of these results currently remains unknown [10]. Since previously reported ZMYM3 mutations appeared to be loss-of-function

mutations and ZMYM3 was shown to promote DNA repair by interacting with BRCA1, ZMYM3 may suppress tumorigenesis [24]. This implication appears to be in contrast to our hypothesis. However, previous studies indicated that ZMYM3 (*Zmym3*) has many functions. *Zmym3* was found to be alternatively spliced in developmental- and tissue-specific manners [33]. Comparisons of RNA profiles between *Zmym3*-knockout spermatogonial stem cells and wild-type spermatogonial cells in mice by an RNA-sequencing analysis revealed the abnormal expression of many genes in *Zmym3*-knockout cells [17]. Multiple ZMYM3 functions have already been reported, such as modifications to histone acetylation and the promotion of DNA repair [14, 24]. To the best of our knowledge, this is the first study to examine the functions of ZMYM3 in human lung carcinomas. As expected, ZMYM3 promoted cell proliferation in human lung cancer. Additionally, our hypothesis is consistent with the results of the immunohistochemical study on adult mouse tissues and human lung carcinomas described above. Therefore, ZMYM3 (*Zmym3*) appears to promote cell proliferation in normal mouse tissues and human lung carcinomas.

ZMYM3 has been shown to promote DNA repair and more meiosis I spermatocytes underwent apoptosis in *Zmym3*-knockout mice than in wild-type mice [17, 24]. These findings imply that the ZMYM3-knockdown in a human lung cancer cell line activates apoptosis through the disruption of DNA repair. However, the results of flow cytometry and the TUNEL assay rejected this proposal.

In conclusion, ZMYM3 may promote cell proliferation in human lung carcinomas, particularly SCLC. Further investigations are needed to clarify the functions of ZMYM3 (*Zmym3*) in tumors.

V. Conflicts of Interest

The authors declare that there are no conflicts of interest.

VI. Acknowledgment

We thank Ms. Takako Maeda and Ms. Yuko Nakaishi-Fukuchi for their technical support. We encountered ZMYM3 when we were investigating tobacco-related molecules in mice exposed to smoking with Dr. Kanako Niimori. The present study was supported in part by a grant from the Smoking Research Foundation, and in part by Grant-in-Aids for Scientific Research from the Ministry of Education, Culture, Sports, Science and Technology of Japan (20H03691).

VII. References

1. Abeshouse, A., Ahn, J., Akbani, R., Ally, A., Amin, S., Andry, A. D., *et al.* (2015) The molecular taxonomy of primary prostate cancer. *Cell* 163; 1011–1025.

2. Alexander, M., Kim, S. Y. and Cheng, H. (2020) Update 2020: management of non-small cell lung cancer. *Lung* 198; 897–907.
3. Alizadeh, F., Bozorgmehr, A., Tavakkoly-Bazzaz, J. and Ohadi, M. (2018) Skewing of the genetic architecture at the ZMYM3 human-specific 5' UTR short tandem repeat in schizophrenia. *Mol. Genet. Genomics* 293; 747–752.
4. Alizadeh, F., Moharrami, T., Mousavi, N., Yazarlou, F., Bozorgmehr, A., Shahsavand, E., et al. (2019) Disease-only alleles at the extreme ends of the human ZMYM3 exceptionally long 5' UTR short tandem repeat in bipolar disorder: a pilot study. *J. Affect. Disord.* 251; 86–90.
5. Aubry, S., Shin, W., Crary, J. F., Lefort, R., Qureshi, Y. H., Lefebvre, C., et al. (2015) Assembly and interrogation of Alzheimer's disease genetic networks reveal novel regulators of progression. *PLoS One* 10; e0120352.
6. Baldin, V., Lukas, J., Marcote, M. J., Pagano, M. and Draetta, G. (1993) Cyclin D 1 is a nuclear protein required for cell cycle progression in G1. *Genes Dev.* 7; 812–821.
7. Carbonari, M., Cibati, M., Cherchi, M., Sbarigia, D., Pesce, A. M., Dell'Anna, L., et al. (1994) Detection and characterization of apoptotic peripheral blood lymphocytes in human immunodeficiency virus infection and cancer chemotherapy by a novel flow immunocytometric method. *Blood* 83; 1268–1277.
8. Gazdar, A. F., Carney, D. N., Russell, E. K., Sims, H. L., Baylin, S. B., Bunn, Jr., P. A., et al. (1980) Establishment of continuous, clonable cultures of small-cell carcinoma of the lung which have amine precursor uptake and decarboxylation cell properties. *Cancer Res.* 40; 3502–3507.
9. Gazdar, A. F., Linnoila, R. I., Kurita, Y., Oie, H. K., Mulshine, J. L., Clark, J. C., et al. (1990) Peripheral airway cell differentiation in human lung cancer cell lines. *Cancer Res.* 50; 5481–5487.
10. George, J., Lim, J. S., Jang, S. J., Cun, Y., Ozretić, L., Kong, G., et al. (2015) Comprehensive genomic profiles of small cell lung cancer. *Nature* 524; 47–53.
11. Gerdes, J., Schwab, U., Lemke, H. and Stein, H. (1983) Production of a mouse monoclonal antibody reactive with a human nuclear antigen associated with cell proliferation. *Int. J. Cancer* 31; 13–20.
12. Giard, D. J., Aaronson, S. A., Todaro, G. J., Arnstein, P., Kersey, J. H., Dosik, H., et al. (1973) In vitro cultivation of human tumors: establishment of cell lines derived from a series of solid tumors. *J. Natl. Cancer Inst.* 51; 1417–1423.
13. Girard, L., Zöchbauer-Müller, S., Virmani, A. K., Gazdar, A. F. and Minna, J. D. (2000) Genome-wide allelotyping of lung cancer identifies new regions of allelic loss, differences between small cell lung cancer and non-small cell lung cancer, and loci clustering. *Cancer Res.* 60; 4894–4906.
14. Hakimi, M.-A., Dong, Y., Lane, W. S., Speicher, D. W. and Shiekhhattar, R. (2003) A candidate X-linked mental retardation gene is a component of a new family of histone deacetylase-containing complexes. *J. Biol. Chem.* 278; 7234–7239.
15. Heck, M. M. S. and Earnshaw, W. C. (1986) Topoisomerase II: a specific marker for cell proliferation. *J. Cell Biol.* 103; 2569–2581.
16. Hiraiwa, A., Fujita, M., Nagasaka, T., Adachi, A., Ohashi, M. and Ishibashi, M. (1997) Immunolocalization of hCDC47 protein in normal and neoplastic human tissues and its relation to growth. *Int. J. Cancer* 74; 180–184.
17. Hu, X., Shen, B., Liao, S., Ning, Y., Ma, L., Chen, J., et al. (2017) Gene knockout of Zmym3 in mice arrests spermatogenesis at meiotic metaphase with defects in spindle assembly checkpoint. *Cell Death Dis.* 8; e2910.
18. Iams, W. T., Porter, J. and Horn, L. (2020) Immunotherapeutic approaches for small-cell lung cancer. *Nat. Rev. Clin. Oncol.* 17; 300–312.
19. Johnson, B. E., Russel, E., Simmons, A. M., Phelps, R., Steinberg, S. M., Ihde, D. C., et al. (1996) MYC family DNA amplification in 126 tumor cell lines from patients with small cell lung cancer. *J. Cell. Biochem. Suppl.* 24; 210–217.
20. Khan, S. A., Amnekar, R., Khade, B., Barreto, S. G., Ramadwar, M., Shrikhande, S. V., et al. (2016) p38-MAPK/MSK1-mediated overexpression of histone H3 serine 10 phosphorylation defines distance-dependent prognostic value of negative resection margin in gastric cancer. *Clin. Epigenetics* 8; 88.
21. Kishimoto, N. (1992) Studies on cell biology and chemotherapy of lung cancer using tissue culture techniques part 2. Biological characteristics of five newly established small cell lung cancer cell lines. *J. Okayama Med. Assoc.* 104; 905–913.
22. Koopman, G., Reutelingsperger, C. P. M., Kuijten, G. A. M., Keehnen, R. M. J., Pals, S. T. and van Oers, M. H. J. (1994) Annexin V for flow cytometric detection of phosphatidylserine expression on B cells undergoing apoptosis. *Blood* 84; 1415–1420.
23. Kubo, T., Yamamoto, H., Lockwood, W. W., Valencia, I., Soh, J., Peyton, M., et al. (2009) MET gene amplification or EGFR mutation activate MET in lung cancers untreated with EGFR tyrosine kinase inhibitors. *Int. J. Cancer* 124; 1778–1784.
24. Leung, J. W. C., Makharashvili, N., Agarwal, P., Chiu, L.-Y., Pourpre, R., Cammarata, M. B., et al. (2017) ZMYM3 regulates BRCA1 localization at damaged chromatin to promote DNA repair. *Genes Dev.* 31; 1–15.
25. Mirski, S. E. L., Gerlach, J. H. and Cole, S. P. C. (1987) Multidrug resistance in a human small cell lung cancer cell line selected in Adriamycin. *Cancer Res.* 47; 2594–2598.
26. Miyachi, K., Fritzler, M. J. and Tan, E. M. (1978) Autoantibody to a nuclear antigen in proliferating cells. *J. Immunol.* 121; 2228–2234.
27. Namdar-Aligoodarzi, P., Mohammadparast, S., Zaker-Kandjani, B., Talebi Kakroodi, S., Jafari Vesiehsari, M. and Ohadi, M. (2015) Exceptionally long 5' UTR short tandem repeats specifically linked to primates. *Gene* 569; 88–94.
28. Nicoletti, I., Migliorati, G., Pagliacci, M. C., Grignani, F. and Riccardi, C. (1991) A rapid and simple method for measuring thymocyte apoptosis by propidium iodide staining and flow cytometry. *J. Immunol. Methods* 139; 271–279.
29. Okamoto-Kubo, S., Nishio, K., Heike, Y., Yohida, M., Ohmori, T. and Saijo, N. (1994) Apoptosis induced by etoposide in small-cell lung cancer cell lines. *Cancer Chemother. Pharmacol.* 33; 385–390.
30. Philips, A. K., Sirén, A., Avela, K., Somer, M., Peippo, M., Ahvenainen, M., et al. (2014) X-exome sequencing in Finnish families with intellectual disability—four novel mutations and two novel syndromic phenotypes. *Orphanet. J. Rare Dis.* 9; 49.
31. Robinson, G., Parker, M., Kranenburg, T. A., Lu, C., Chen, X., Ding, L., et al. (2012) Novel mutations target distinct subgroups of medulloblastoma. *Nature* 488; 43–48.
32. Sato, Y., Matsuo, A., Kudoh, S., Liu, F., Hasegawa, K., Shinmyo, Y., et al. (2018) Expression of Draxin in lung carcinomas. *Acta Histochem. Cytochem.* 51; 53–62.
33. Scheer, M. P., van der Maarel, S., Kübart, S., Schulz, A., Wirth, J., Schweiger, S., et al. (2000) DXS6673E encodes a predominantly nuclear protein, and its mouse ortholog DXHXS6673E is alternatively spliced in a developmental- and tissue-specific manner. *Genomics* 63; 123–132.
34. Sgonc, R. and Gruber, J. (1998) Apoptosis detection: an overview. *Exp. Gerontol.* 33; 525–533.
35. Shen, H., Chen, Z., Ding, X., Qi, X., Cen, J., Wang, Y., et al. (2014) BMI1 reprogrammes histone acetylation and enhances c-

- fos* pathway via directly binding to *Zmym3* in malignant myeloid progression. *J. Cell. Mol. Med.* 18; 1004–1017.
36. Siegel, R. L., Miller, K. D. and Jemal, A. (2020) Cancer Statistics, 2020. *CA Cancer J. Clin.* 70; 7–30.
 37. Takase, Y., Naito, Y., Okabe, Y., Ishida, Y., Yamaguchi, T., Abe, H., *et al.* (2019) Insulinoma-associated protein 1 expression in pancreatic neuroendocrine tumours in endoscopic ultrasound-guided fine-needle aspiration cytology: An analysis of 14 patients. *Cytopathology* 30; 194–200.
 38. Taniguchi, A., Susa, T., Kogo, H., Iizuka-Kogo, A., Yokko, S. and Matsuzaki, T. (2019) Long-term pilocarpine treatment improves salivary flow in irradiated mice. *Acta Histochem. Cytochem.* 52; 45–58.
 39. Tirode, F., Surdez, D., Ma, X., Parker, M., Le Deley, M. C., Bahrami, A., *et al.* (2014) Genomic landscape of Ewing sarcoma defines an aggressive subtype with co-association of *STAG2* and *TP53* mutations. *Cancer Discov.* 4; 1342–1353.
 40. Todorov, I. T., Werness, B. A., Wang, H.-Q., Buddharaju, L. N., Todorova, P. D., Slocum, H. K., *et al.* (1998) HsMCM2/BM28: a novel proliferation marker for human tumors and normal tissues. *Lab. Invest.* 78; 73–78.
 41. Travis, W. D., Brambilla, E., Burke, A. P., Marx, A. and Nicholson, A. G. (2015) WHO Classification of Tumours of the Lung, Pleura, Thymus and Heart, 4th ed., International Agency for Research on Cancer, Lyon.
 42. van der Maarel, S. M., Scholten, I. H. J. M., Huber, I., Philippe, C., Suijkerbuijk, R. F., Gilgenkrantz, S., *et al.* (1996) Cloning and characterization of *DXS6673E*, a candidate gene for X-linked mental retardation in Xq13.1. *Hum. Mol. Genet.* 5; 887–897.
 43. Wang, L., Lawrence, M. S., Wan, Y., Stojanov, P., Sougnez, C., Stevenson, K., *et al.* (2011) *SF3B1* and other novel cancer genes in chronic lymphocytic leukemia. *N. Engl. J. Med.* 365; 2497–2506.
 44. Yoshioka, S., King, M. L., Ran, S., Okuda, H., MacLean, J. A., McAsey, M. E., *et al.* (2012) WNT7A Regulates Tumor Growth and Progression in Ovarian Cancer through the WNT/b-Catenin Pathway. *Mol. Cancer Res.* 10; 469–482.

This is an open access article distributed under the Creative Commons License (CC-BY-NC), which permits use, distribution and reproduction of the articles in any medium provided that the original work is properly cited and is not used for commercial purposes.
